Check for updates

Liquid crystal gelators with photo-responsive and AIE properties†

Xia Yu,‡[a] Hui Chen, [ID] ‡[b] Xiang Shi,[c] Pierre-Antoine Albouy,[c] Jia Guo,[a] Jun Hu [ID] *[a] and Min-Hui Li [ID] *[ab]

A series of new liquid crystal (LC) gelators with photo-responsive and AIE properties were synthesized by connecting cholesterol and tetraphenylethylene (TPE) to a central azobenzene moiety (**trans-C$_n$-Chol**, n = 0, 1, 3, 5), in which alkyl chains with different lengths (CH$_2$)$_n$ were used as spacer to adjust the distance between cholesterol and azobenzene, while a fixed alkyl chain (CH$_2$)$_6$ was placed between azobenzene and TPE. All these **trans-C$_n$-Chol** molecules exhibit LC phase of type smectic A. Three derivatives of **trans-C$_n$-Chol** (with n = 0, 1, 3) keep their smectic A LC phases at room temperature upon cooling after at least one heating history to isotropic (Iso) phase, and present hot-crystallization (94–104 °C) upon further heating. Moreover, their thin films with LC state at room temperature can undergo photo-responsive LC–Iso phase transition under UV irradiation because of the *trans–cis* photo-isomerization of azobenzene. On the other hand, as gelators **trans-C$_n$-Chol** with long spacers, **trans-C$_3$-Chol** and **trans-C$_5$-Chol**, form stable low-molecular weight organogels (LMOGs) in various solvents, whereas **trans-C$_0$-Chol** and **trans-C$_1$-Chol** with short spacers cannot form stable LMOGs in tested solvents. Diverse supramolecular chiral structures like "sea urchins", helical fibers, "honeycomb" and twisted ribbons were observed for both **trans-C$_3$-Chol** and **trans-C$_5$-Chol** gels. On account of the involvement of TPE and azobenzene moieties, these molecules present significant aggregation-induced emission (AIE) and gel-enhanced emission, and their LMOGs exhibit photo-responsive gel–sol transition. These LC molecules with gelation ability, AIE characteristics and photo-responsive properties can have potential applications as sensors and optoelectronic materials.

Introduction

Low-molecular weight organogels (LMOGs) are engineered by the assembly of small molecules *via* the synergistic effect of non-covalent interactions, thus driving the formation of three-dimensional networks from fibrous, tubular, rod- or ribbon-like structures.[1–3] As one of the ideal blocks in LMOGs, cholesterol is widely used in the fabrication of intelligent gels by intro-ducing functional groups on its backbone.[4–8] Of them, the

[a] *Beijing Advanced Innovation Center for Soft Matter Science and Engineering, Beijing University of Chemical Technology, Beijing 100029, China. E-mail: limh@mail.buct.edu.cn, jhu@mail.buct.edu.cn*

[b] *Chimie ParisTech, PSL University Paris, CNRS, Institut de Recherche de Chimie Paris, 75005 Paris, France. E-mail: min-hui.li@chimieparistech.psl.eu*

[c] *Université Paris-Sud, CNRS, Laboratoire de Physique des Solides, UMR8502, 91405 Orsay Cedex, France*

† Electronic supplementary information (ESI) available: Synthetic route, MS and NMR spectra of *trans*-C$_n$-Chol and their intermediates; DSC data for phase transition temperature of *trans*-C$_n$-Chol; SAXS, WAXS and POM of *trans*-C$_0$-Chol; SAXS, WAXS and XRD of *trans*-C$_5$-Chol; stretched length of *trans*-C$_n$-Chol; gel ability in different solvents; SEM images of *trans*-C$_3$-Chol; CD spectra of *trans*-C$_3$-Chol and *trans*-C$_5$-Chol; fluorescence, UV-Vis and NMR spectra of *trans*-C$_3$-Chol for AIE and photo-responsive characteristic. See DOI: 10.1039/c8qm00340h

‡ These authors contributed equally to this work.

photo-responsive LMOG is quite interesting due to its clean, fast, controlled and anti-fatigue features.[4,9,10] To date a number of photo-sensitive units like azobenzene, spiropyran, and dithienylethene have been incorporated in the cholesteric LMOGs.[4,5,11] For example, Feringa and co-workers reported a photo-triggered reversible transition between organogels and vesicles using the amphiphilic dithienylethene, functionalized with a cholesterol and a poly(ethylene glycol)-modified pyridinium,[11] while Zhu's group developed a multi-stimuli responsive organogel by featuring tetrathiafulvalene (TTF) and azobenzene groups. Its gel–sol transition could be reversibly tuned by either manipulating the redox state of TTF or utilizing the photoisomerization of azobenzene.[4] Recently, luminogens with aggregation-induced emission (AIE) characteristics have also been introduced into LMOGs that show features of gelation-enhanced emission.[12,13] For example, the groups of Wang and Ma have prepared AIE LMOGs by connecting tetraphenylethylene (TPE) and cholesterol moieties to a central salicylideneaniline.[13] Their systems allow one to make use of the Excited-State Intra-molecular Proton Transfer (ESIPT) process with large Stokes shift in gel state.

In this research, we report on new liquid crystal LMOGs with photo-responsive and AIE properties by integrating cholesterol
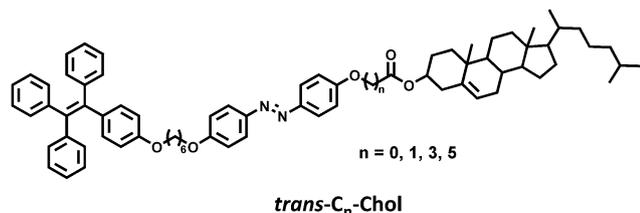
This journal is © The Royal Society of Chemistry and the Chinese Chemical Society 2018

Mater. Chem. Front., 2018, **2**, 2245–2253 | 2245

Scheme 1   Molecular structure of *trans*-C*n*-Chol.

(gelator), azobenzene (photosensitive unit) and TPE (AIEgen) in one molecule (see Scheme 1). It needs to be noted that besides the involvement in gelation and photo-responsive features, both cholesterol and azobenzene are liquid crystal (LC) units.[14–16] Thus, the research of the LC properties of these LMOGs when conjugating non-rod-like blocks like TPE is also of great importance.

A series of functional gelators, *trans*-C*n*-Chol, as shown in Scheme 1, were synthesized (see Experimental section) and their properties studied in detail. Alkyl chains with different lengths were utilized to adjust the distance between cholesterol and azobenzene moieties, and an alkyl chain with fixed length $(CH_2)_6$ was used as spacer between azobenzene and TPE. The whole series of *trans*-C*n*-Chol exhibit LC phase of type smectic A (SmA). *trans*-C$_0$-Chol and *trans*-C$_3$-Chol exhibit the enantiotropic SmA phase on heating and cooling, while *trans*-C$_1$-Chol and *trans*-C$_5$-Chol show the monotropic SmA phase on cooling. On the other hand, *trans*-C$_3$-Chol and *trans*-C$_5$-Chol can be gelled in single and mixed solvents, whereas *trans*-C$_0$-Chol and *trans*-C$_1$-Chol cannot form gels. These LMOGs not only have the chiral assembled morphologies, but also exhibit significantly enhanced emission during the gelation process. Finally, the resulting fluorescent LMOGs display a photo-sensitive gel–sol transition. Our work has provided smart LC gelators with AIE and photo-responsive properties, which have promising applications in sensors and optoelectronic materials.

Results and discussion

Liquid crystal behaviours

The liquid crystal behaviours of the whole series were studied in detail by differential scanning calorimetry (DSC), polarizing optical microscopy (POM), and small angle and wide angle X-ray scattering (SAXS and WAXS). Their DSC thermograms are shown in Fig. 1, where *trans*-C$_0$-Chol and *trans*-C$_3$-Chol exhibit enantiotropic LC phase upon heating and cooling, while *trans*-C$_1$-Chol and *trans*-C$_5$-Chol show monotropic LC phase only upon cooling.

We discuss the case of *trans*-C$_0$-Chol firstly. Upon heating at 2 °C min^{-1}, the first small peak at around 161 °C corresponds to a re-organization in the crystal phase. The melting of crystal phase (Cr) occurs at 175 °C and a LC phase exists in a narrow range from 175 to 178 °C (also confirmed by a slow DSC scan at 0.5 °C min^{-1}, Fig. S1, ESI†). However upon cooling from isotropic phase (Iso) the LC phase persists until room temperature without recrystallization, probably because of the low
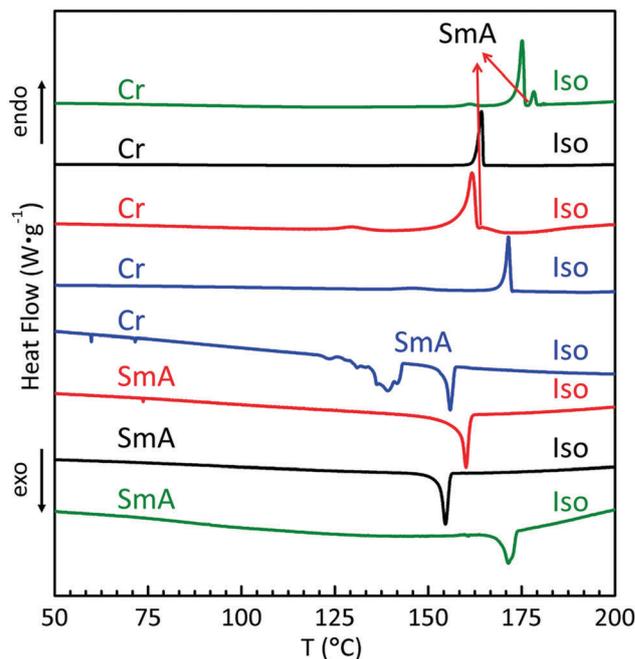

Fig. 1   DSC thermograms of *trans*-C$_0$-Chol (green lines), *trans*-C$_1$-Chol (black lines), *trans*-C$_3$-Chol (red lines) and *trans*-C$_5$-Chol (blue lines) upon the first heating (4 upper curves) and first cooling (4 lower curves) cycle at a rate of 2 °C min^{-1}. Samples are solids obtained by recrystallization after synthesis.

mobility of *trans*-C$_0$-Chol and the consequent supercooling of LC phase. The phase transition temperatures and enthalpies are summarized in Table S1 (ESI†). The textures of LC phase observed by POM are shown in Fig. 2A. The typical fan-shaped (focal conic) textures indicate a smectic A (SmA) phase for *trans*-C$_0$-Chol. This was confirmed finally by SAXS and WAXS as shown in Fig. S2 (ESI†) and Table 1. A smectic spacing of
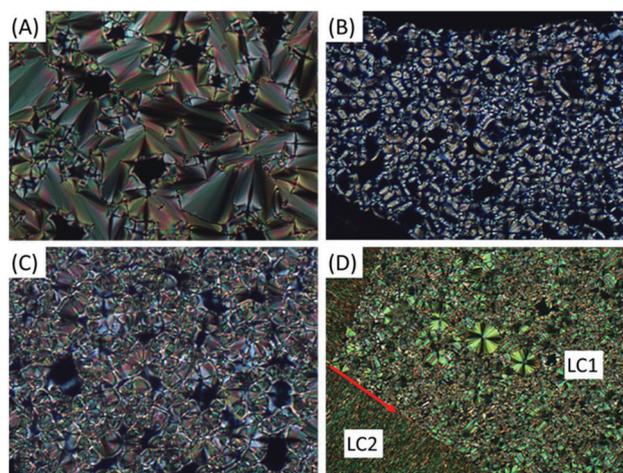

Fig. 2   Textures of *trans*-C*n*-Chol observed by POM upon cooling from isotropic phase. (A) *trans*-C$_0$-Chol at 25 °C; (B) *trans*-C$_1$-Chol at 25 °C; (C) *trans*-C$_3$-Chol at 25 °C; (D) *trans*-C$_5$-Chol at 145 °C (the second phase LC2 started to grow from the left side). These typical fan-shaped textures indicate SmA phase. In (D) LC1 is SmA, while LC2 is a crystalline phase (see text).

Table 1 Smectic spacing of **trans-C_n-Chol** upon cooling from isotropic phase

Sample	**trans-C_0-Chol** (RT)	**trans-C_1-Chol** (RT)	**trans-C_3-Chol** (RT)	**trans-C_5-Chol** (150 °C)
d (nm)	5.63	5.85	6.01	6.35

5.63 nm and an average lateral distance of 0.47 nm between molecules were measured. Interestingly, hot-recrystallization was observed at around 94 °C upon the second heating, which is facilitated by the increase of molecular mobility (Fig. S3, ESI†). At around 175 °C, the melting from crystal to LC phase and the transition from LC phase to isotropic phase are merged in a large peak in the DSC curve. Nevertheless, the SmA phase was actually observed by POM upon a very slow heating (Fig. S4, ESI†). In summary, the phase sequence of **trans-C_0-Chol** is Cr-175.1 °C-SmA-178.3 °C-Iso upon heating and Iso-171.5 °C-SmA upon cooling.

Very similar phase behaviours were observed for **trans-C_3-Chol** (Fig. 1, 2, Fig. S3 and Table S1, ESI†) with phase sequence Cr-161.7 °C-SmA-164.7 °C-Iso upon heating and Iso-160.1 °C-SmA upon cooling. The smectic spacing measured by SAXS is 6.01 nm (Table 1).

In contrast, **trans-C_1-Chol** exhibits monotropic LC phase with phase sequence Cr-164.2 °C-Iso upon heating and Iso-154.6 °C-SmA upon cooling (Fig. 1, 2, Fig. S3 and Table S1, ESI†). The smectic spacing measured by SAXS is 5.85 nm (Table 1).

The LC phase of **trans-C_5-Chol** is also monotropic, but two phase transitions instead of one were observed with phase sequence Cr-171.5 °C-Iso upon heating and Iso-155.9 °C-SmA-139.1 °C-LC2 upon cooling (Fig. 1, 2, Fig. S3 and Table S1, ESI†). Fig. 2D shows the textures of SmA and LC2 phase at 145 °C, where the growth of LC2 (left, slightly cooler than the center, marked by an arrow) is observable under POM. By performing SAXS in SmA phase at 150 °C after the first heating to isotropic phase (180 °C), a smectic spacing of 6.35 nm was measured (Table 1). In order to get more information on the structure of LC2 phase, we tried to align **trans-C_5-Chol** and performed X-ray diffraction. The sample was introduced in a flat capillary at 150 °C after having first heated to isotropic phase (180 °C), and then was cooled down to room temperature for SAXS and WAXS experiments (Fig. S5 and Table S2, ESI†). SAXS revealed a periodical distance of 6.09 nm with 4 orders of diffraction visible and a certain orientation. Meanwhile, WAXS revealed the crystalline structures. Thus the LC2 phase is a smectic phase with crystalline orders in the smectic layer. The enthalpy of SmA–LC2 transition is also similar to that of Cr–SmA transition for **trans-C_3-Chol** (see Table S1, ESI†). Therefore, **trans-C_5-Chol** with long spacer has sufficient molecular mobility so that the re-crystallization takes place in a normal way upon cooling.

Notably, the period d of SmA phase of each derivative in the whole series (d = 5.63, 5.85, 6.01 and 6.35 nm) corresponds to a value between l and $2l$, l being the stretched length of each molecule (l = 4.74, 4.95, 5.26 and 5.52 nm) as determined with a molecular model (Fig. S6A–D, ESI†). Therefore, all molecules of

trans-C_n-Chol exhibit an interdigitated antiparallel bilayer smectic A phase (SmA$_d$). This is also comprehensible from the major difference of molecular areas between the TPE subunit (clover-like) and azobenzene/cholesterol parts (rod-like), which prevents the single layer organization. The non-flexible and non-rod-like tetraphenylethylene (TPE) fitted finally into the wholly rod-like molecules and didn't destroy their LC properties. A possible model of molecular organization of SmA$_d$ is proposed in Fig. S6E (ESI†). We noticed also interestingly that three samples in the series (**trans-C_0-Chol**, **trans-C_1-Chol** and **trans-C_3-Chol**) presented hot-crystallization (94–104 °C) upon second or further heating. As re-crystallization will introduce significant texture changes and structure modification in the aligned LC samples, this hot recrystallization can be used to design sensors to trace thermal history experienced by materials.

Gelation ability

In general, the procedure of the gelation test was as follows: a solution of **trans-C_n-Chol** at a typical concentration of c = 60 mg mL^{-1} in a given solvent was heated in a sealed bottle until a clear solution formed. After that, it was cooled down to room temperature. The gel state was evaluated by the "stable to inversion of a test tube" method,[17] and the results are summarized in Table S3 (ESI†). As can be seen, **trans-C_5-Chol** and **trans-C_3-Chol** form gels in dimethylformamide (DMF), acetone, ethyl acetate (EA) and dichloromethane/ethyl acetate (DCM/EA), respectively, while **trans-C_0-Chol** and **trans-C_1-Chol** cannot turn into gel in any of the above solvents, suggesting that the flexible spacer should play a crucial role in the gel formation.[18]

Gel morphologies

The morphologies of these gels were studied by using a scanning electron microscope (SEM). It can be seen that **trans-C_5-Chol** molecules assemble into various chiral structures, *i.e.* twisted ribbons in DMF (Fig. 3A), "sea urchins" in acetone (Fig. 3B), "flowers" in EA (Fig. 3C) and helical fibers in DCM/EA (Fig. 3D). Their length and width are several micrometres, and their helical structures are pointed out by arrows in SEM images. Similarly, the micro-scale chiral structures of "honeycomb", twisted ribbons, helical fibers and "sponge" assembled by **trans-C_3-Chol** were obtained in DMF, acetone, EA and DCM/EA, respectively (Fig. S7, ESI†). Their supramolecular chirality can be further confirmed by circular dichroism (CD) spectroscopy (Fig. S8, ESI†). As can be seen, there is no Cotton effect for both **trans-C_5-Chol** and **trans-C_3-Chol** when they are completely dissolved in tetrahydrofuran (THF), revealing the existence of free molecules; conversely, strong CD signals are measured for the gels of **trans-C_5-Chol** and **trans-C_3-Chol**, indicating the formation of chiral assemblies.[19] It should be noted that the **trans-C_5-Chol** gel exhibits a broad CD signal extending to the near infrared (NIR) region, which might be due to the light scattering caused by the aggregation.[20,21] Considering the abundance of chiral cholesterol in the gelator, it is postulated that the molecular chirality of **trans-C_5-Chol** and **trans-C_3-Chol** is amplified and expressed at the supramolecular level. During these processes,
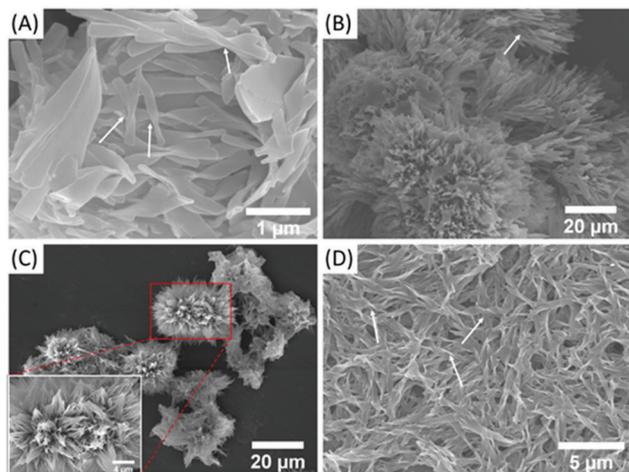
Fig. 3 SEM images of *trans*-C$_5$-Chol in (A) DMF, (B) acetone, (C) EA and (D) DCM/EA (1/2, v/v); inset: partial enlarged view.

Fig. 4 (A) Fluorescence spectra of *trans*-C$_5$-Chol in DCM/EA (c = 56 mM) at different fractions of EA; (B) plots of I/I_0 of *trans*-C$_5$-Chol as a function of EA fraction in DCM/EA. I_0 = fluorescence peak intensity in DCM; I = fluorescence peak intensity in DCM/EA with different volume fractions; (C) temperature-dependent fluorescence spectra of *trans*-C$_5$-Chol gel in DMF (c = 30 mM); (D) plots of I/I_{80} of *trans*-C$_5$-Chol gel as a function of temperature from 25 to 80 °C. I_{80} = fluorescence peak intensity at 80 °C, I = fluorescence peak intensity at other temperatures (25, 35, 45, 55, 65 and 75 °C). λ_{Ex} = 310 nm.

π-stacking was found to be the major driving force by exploring temperature-dependent ^{1}H NMR experiments. As shown in Fig. S9 (ESI†), protons of azobenzene and TPE groups (H1, H2, H3) shift up-field gradually with the increase in temperature, revealing the presence of π-stacking in these gels.[22]

AIE characteristics

The AIE characteristics of *trans*-C$_5$-Chol and *trans*-C$_3$-Chol were first evaluated by a standard experiment on studying their fluorescence behaviours in mixtures of good and poor solvents (DCM/EA) with different solvent volume ratio. As shown in Fig. 4A, *trans*-C$_5$-Chol is completely soluble in DCM and only fairly weak fluorescence is observed upon excitation at 310 nm. Along with the gradual increase of the EA (poor solvent) fraction to 93%, the mixture becomes emissive at 531 nm since the solvating power has been decreased to an extent that the molecules start to aggregate. When the EA fraction is 97%, the fluorescence intensity is increased by up to 66 times compared to that in pure DCM (Fig. 4B). It is mainly attributed to the limited rotation of the single bond between phenyl ring and olefin, which causes the excited state energy back to the ground state through the radiative channel. Similar AIE phenomena were observed for *trans*-C$_3$-Chol. As shown in Fig. S10A (ESI†), a dramatic enhancement in emission intensity at 533 nm occurs when the volume ratio of EA becomes >94%. The fluorescence intensity at 98% of EA volume ratio is 82 times stronger than that in pure DCM (Fig. S10B, ESI†).

We examined then the fluorescence change along with gel–sol transformation as a function of temperature. As shown in Fig. 4C, *trans*-C$_5$-Chol gel at 25 °C is fluorescent because of the aggregated ribbon-like nanostructures (Fig. 3A). Then its fluorescence intensity at 573 nm decreases gradually upon heating from 25 to 80 °C, and at 80 °C the intensity value is only 1/16 of that at 25 °C (Fig. 4D). This fluorescence intensity decrease is associated to the gel–sol transformation upon heating along with at least partial disassembly of nanostructures. A similar fluorescence change along with gel–sol transformation
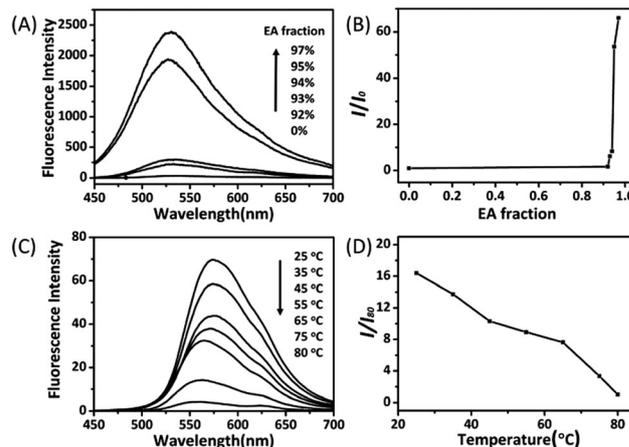
upon heating was observed for *trans*-C$_3$-Chol gel in DMF, except that an abrupt decrease of the fluorescence intensity occurred as the gel was heated to 65 °C and then remained stable and low until 80 °C (Fig. S10C and D, ESI†). It should be noted that in comparison with the emission peak in DCM/EA with the maximum at 531 nm (or 533 nm), the emission peak in DMF was red-shifted, which may be caused by the difference in solvent polarity. Similar results have been reported by Tang and co-workers in 2014, where the emission peak of TPE derivatives shifted to the long wavelength when the solvent was changed from apolar toluene to polar acetonitrile.[23] On the basis of the above discussion, we can conclude that both *trans*-C$_3$-Chol and *trans*-C$_5$-Chol are AIE active gelators.

He and co-workers have also connected TPE with azobenzene in their colloid and polymer systems.[24,25] However, their azobenzene moieties are push–pull type with absorption at wavelength from 400 to 500 nm. Therefore their systems don't show any fluorescence due to the fluorescence resonance energy transfer (FRET) process, where the fluorescent states of TPE parts (with excitation at around 365 nm and emission at around 470 nm) are well quenched by push–pull azobenzene moieties. Interestingly, the AIE fluorescence of TPE can be restored by the reduction of azobenzene to hydrazobenzene upon treatment with hydrazine hydrate.[25] But the AIE fluorescence recovery is at the cost of the loss of photo-responsive properties of azobenzene.

Photo-responsive properties

In our systems, *trans*-C$_3$-Chol and *trans*-C$_5$-Chol are not only fluorescent with aggregation-induced emission and gelation-enhanced emission as discussed above, but also form photo-responsive gels because of the presence of the azobenzene

moiety (normal type). Their gel–sol transition can be triggered by UV light. As shown in Fig. 5A, upon UV light (365 nm) irradiation of 15 min (900 s), the **trans-C₅-Chol** gel in DMF collapses to become liquid-like with the colour changing from yellow to orange. The photo-triggered gel–sol transition of **trans-C₅-Chol** and **trans-C₃-Chol** was then investigated by UV-Vis spectroscopy, ^{1}H NMR spectra, SEM and CD spectra.

trans-C₅-Chol and **trans-C₃-Chol** show, in DMF solution, a strong UV absorption band centered at around 360 nm and a shoulder around 450 nm (Fig. 5B and Fig. S11, ESI†) which corresponded to π–π* and n–π* electron transition, respectively.[26] Upon irradiation of UV light at 365 nm, the absorbance at 360 nm decreased from 1.45 to 0.21, while the weak absorbance at 450 nm increased to 0.15. Therefore, both **trans-C₅-Chol** and **trans-C₃-Chol** in DMF solution undergo *trans–cis* photoisomerization of azobenzene upon irradiation at 365 nm in the π–π* absorption region.

Interesting information on the photoisomerization of gels was recorded in ^{1}H NMR experiments. As shown in Fig. 6, upon irradiation of UV light until 460 s, proton signals (C₃-H1, C₃-H2) belonging to the azobenzene group and the signals of methylene groups linked to azobenzene at 4.13–4.22 ppm (C₃-H4, C₃-H5) in *trans*-configuration undergo significant changes. C₃-H1 and C₃-H2 signals shift toward up-field from 7.89–7.91 to 6.91–6.92 ppm becoming C₃-H1′ and C₃-H2′, meanwhile C₃-H4 and C₃-H5 also move to up-field from 4.13–4.22 ppm to 4.07–3.99 ppm (C₃-H4′, C₃-H5′). These signal changes reveal the *trans* to *cis*-photoisomerization.[27] The isomerization conversion was calculated to be 80% after 460 s of irradiation using the integration area of *trans*-C₃-H3 in cholesterol as the standard. Similar ^{1}H NMR signal evolution was observed for the *trans*- to *cis*-photoisomerization of **trans-C₅-Chol** with a conversation around 58% after 310 s (see Fig. S12, ESI†). Interestingly, we also note that the signals (C₃-H1, C₃-H2) of the *trans*-isomer become significantly shaper after just 30 s of irradiation. We explain this by the fact that the appearance of a few *cis*-isomers (~5%) in the gel could increase the solvent penetration and thus the molecular mobility because the *cis*-isomer is more polar and soluble in DMF. Obviously, **trans-C₅-Chol** and **trans-C₃-Chol** gels can undergo photoisomerization upon UV irradiation, which induced consequently gel–sol transition.
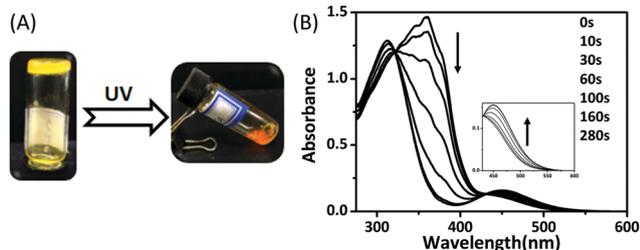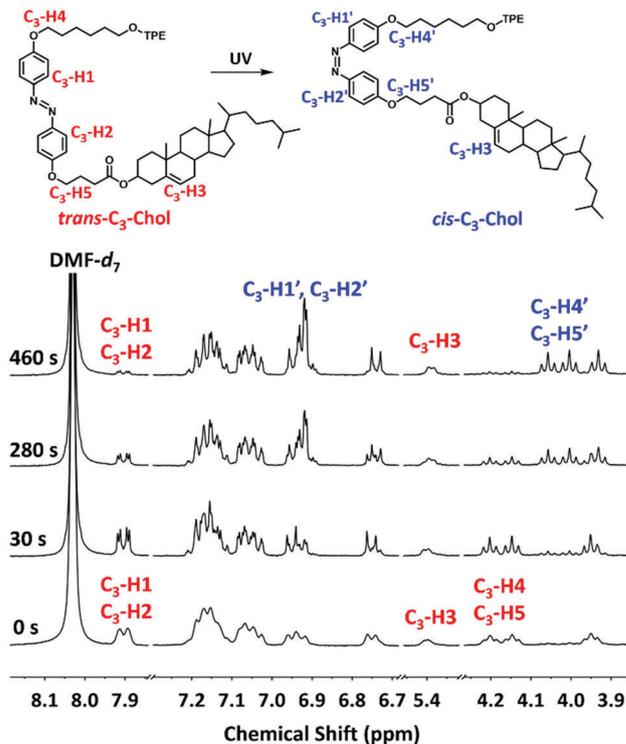
Fig. 6   ^{1}H NMR (400 MHz) of **trans-C₃-Chol** gel in DMF-d_7 (c = 0.45 mM) under UV irradiation at 365 nm (0.25 mW cm⁻²) as a function of irradiation time.

This photoisomerization is further confirmed by its effect on the morphologies and the supramolecular chirality. As shown in Fig. S13 (ESI†), after UV irradiation, the residues of the collapsed gel of **trans-C₃-Chol** become irregular small particles (Fig. S13C, ESI†) in contrast to the "honeycomb" structures in the original gel (Fig. S13A, ESI†). Similarly, the twisted ribbons of the gel of **trans-C₅-Chol** (Fig. S13B, ESI†) break in irregular pieces upon UV irradiation (Fig. S13C and D, ESI†). In addition, no obvious CD signals were detected for the collapsed gels after irradiation as shown in Fig. S8 (ESI†), which means that the supramolecular chiral structures have been destroyed.[28,29]

We have also studied the photo-responsive properties of the series **trans-Cₙ-Chol** (n = 0, 1, 3) in the pure and liquid crystalline state at room temperature. In these molecules, a rod-like mesogen (cholesterol) and a clover-like non-mesogen (TPE) are connected to a central photosensitive mesogen (azobenzene) that can transform from rod-like (mesogen) to banana-like (non-mesogen) due to the *trans–cis* photoisomerization. Thus it is interesting to check whether this shape change in azobenzene can induce the LC–Iso phase transition in **trans-Cₙ-Chol**. A thin film sample was prepared by spin-coating a **trans-Cₙ-Chol** solution (5 mg mL⁻¹ in chloroform at 2000 rounds per min) on a glass plate, which was covered with rubbed polyvinyl alcohol (PVA) known to promote planar alignment of mesogens. The thickness of the sample film is estimated as <500 nm.[30] The sample film placed under a mask, consisting of several parallel transparent stripes, was then exposed to UV light (365 nm, 70 mW cm⁻²) for 60 min (see Fig. 7A and Fig. S14, ESI†).

Fig. 5   (A) Photos showing gel–sol transition of **trans-C₅-Chol** in DMF (c = 62 mM) after 15 min of UV irradiation (90 mW cm⁻², 365 nm). (B) UV-Vis spectra of **trans-C₅-Chol** in DMF solution (c = 0.1 mM) with different UV irradiation time (0.25 mW cm⁻², 365 nm).
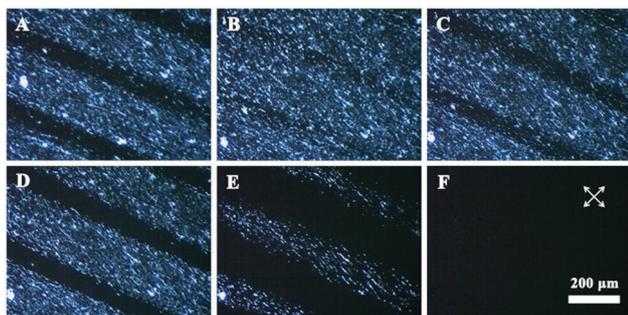
This journal is © The Royal Society of Chemistry and the Chinese Chemical Society 2018

Mater. Chem. Front., 2018, **2**, 2245–2253 | **2249**

Fig. 7 (A) POM photograph of the ***trans*-C$_1$-Chol** film (on a PVA-treated glass plate) after UV irradiation under the mask (width of strip: 50 μm; distance between two stripes: 200 μm) at room temperature. The irradiated parts (stripes) are isotropic, while the masked parts remain in smectic LC phase with birefringence. UV wavelength: 365 nm; UV intensity: 70 mW cm^{-2}; duration: 60 min. (B) The sample (A) heated at 10 °C min^{-1} to T = 120 °C, and the same texture until T = 150 °C. (C) The sample heated further to T = 160 °C. (D) T = 165 °C. (E) Keeping T = 165 °C for 1 min. (F) The sample heated further to T = 166 °C. See text for the discussion on (B–F). Crossed polarizers and scale bar shown in (F) are common for all images.

Fig. 7A shows the POM photograph of the ***trans*-C$_1$-Chol** film irradiated under these conditions between crossed polarizers. It demonstrates clearly that the irradiated parts (stripes) are isotropic, because they are dark and without texture. When rotating the sample platform between crossed polarizers, no change was observed in the irradiated stripes, while bright and dark textures were successively observed in the non-irradiated parts. We can conclude that in the film of ***trans*-C$_n$-Chol** (n = 0, 1, 3), LC–Iso phase transition can be effectively induced by the *trans–cis* photoisomerization of the azobenzene units. The printed stripe pattern is stable and remains unchanged in the dark after one day (time interval after which the sample was reexamined). That means in the sample films the *cis–trans* thermal return doesn't take place at room temperature at least within 24 h, even though *trans*-azobenzene is thermodynamically more stable than *cis*-azobenzene. We then heated the sample at 10 °C min^{-1} to check the *cis–trans* thermal return of azobenzene at higher temperatures. Below 100 °C no significant changes were recorded, while above around 100 °C the isotropic stripes became birefringent, as shown in Fig. 7B for the textures at T = 120 °C–150 °C. This can be explained by the *cis–trans* thermo-isomerization of azobenzene and the reestablishment of the LC phase. Note that we have not observed here the hot-recrystallization in the *trans*-azobenzene domains at T = 100–120 °C as found in the bulk sample (Fig. S3, ESI†), which may be due to the very thin thickness of the sample film. Interestingly, upon further heating to T = 160 °C, the dark stripes reappear (Fig. 7C) and become more and more clearly defined until T = 165 °C (Fig. 7D). When the temperature is maintained at T = 165 °C for 1 min, the bright textures without irradiation start to transform into dark (isotropic) progressively (Fig. 7E). On further heating to T = 166 °C, all domains become isotropic (Fig. 7F). As the heating process (10 °C min^{-1}) is rather rapid here, the *cis–trans* thermal return of azobenzene may be only partial and not complete. The presence of a certain

percentage of non-mesogen with *cis*-azobenzene in the stripes renders the LC–Iso transition temperature of the molecules in the stripes lower than that of pure *trans*-molecules outside the stripes (without irradiation). That's why the LC–Iso transition takes place first in the stripes. Because of these photo- and thermal-responsive phase transitions, the ***trans*-C$_n$-Chol** thin films would be an interesting system for optical image storage, and further developmental investigation would be beneficial.

Conclusion

In summary, we have synthesized a series of functional gelators (***trans*-C$_n$-Chol**, n = 0, 1, 3, 5) with different alkyl spacer length (CH$_2$)$_n$ between cholesterol and azobenzene units. Tetraphenylethylene (TPE), the emblematic AIEgen, was attached to azobenzene with a fixed alkyl spacer (CH$_2$)$_6$. All these ***trans*-C$_n$-Chol** molecules exhibit, in pure state, smectic A LC phases, which are enantiotropic for ***trans*-C$_0$-Chol** and ***trans*-C$_3$-Chol**, but monotropic for ***trans*-C$_1$-Chol** and ***trans*-C$_5$-Chol**. The non-flexible and non-rod-like TPE fits well into the wholly rod-like molecules and doesn't destroy their LC properties. Three samples in the series (***trans*-C$_0$-Chol**, ***trans*-C$_1$-Chol** and ***trans*-C$_3$-Chol**) keep their smectic A LC phases at room temperature upon cooling after at least one heating history to isotropic phase, and present hot-crystallization (94–104 °C) upon the second or further heating. Consequently, the significant texture changes due to hot-recrystallization in the aligned LC samples can be used to design sensors to trace thermal history experienced by materials. Moreover, their thin films with LC state at room temperature can undergo photo-responsive LC–Iso phase transition under UV irradiation. If masks with patterns (*e.g.*, stripes) are applied, the writing–erasing process can be realized by photo- and thermal treatment. Because of these photo- and thermo-responsive phase transitions, the ***trans*-C$_n$-Chol** thin films could be explored as an interesting system for optical image storage.

On the other hand, ***trans*-C$_3$-Chol** and ***trans*-C$_5$-Chol** form stable gels in appropriate solvents or solvent mixtures, while ***trans*-C$_0$-Chol** and ***trans*-C$_1$-Chol** cannot form gels in a large number of solvents tested. During the gelation process, diverse supramolecular chiral structures like "sea urchins", helical fibers, "honeycomb" and twisted ribbons are observed for both ***trans*-C$_3$-Chol** and ***trans*-C$_5$-Chol** gels. These supramolecular chiral structures should stem from the chiral nature of cholesterol. However, in pure state the cholesterol chirality is not expressed in the LC phases, and only smectic A phase is present as previously reported for other cholesterol-based mesogens with different flexible tails.[31–33] The translation of chiral structures from molecular level to supramolecular level is a fascinating subject that we pursue in our future research.

Due to the involvement of the TPE moiety, both ***trans*-C$_3$-Chol** and ***trans*-C$_5$-Chol** LMOGs have significantly enhanced emission induced by molecular self-assembly into fibril or ribbon-like nanostructures. In addition, these LMOGs exhibit the photo-responsive gel–sol transition because of the *trans–cis*

2250 | *Mater. Chem. Front.*, 2018, **2**, 2245–2253

This journal is © The Royal Society of Chemistry and the Chinese Chemical Society 2018

photoisomerization of the azobenzene moiety present in the centre of the molecule. These photo-responsive AIE-active LC gelators may have promising applications in sensors and optoelectronic materials.

Experimental section

Materials

Cholesteryl chloroformate was purchased from Alfa Aesar. All the other chemicals were purchased commercially. Toluene and THF were freshly distilled over sodium with the use of diphenyl ketone as an indicator under nitrogen. Column chromatography was performed with silica gel (200–300 mesh) and all yields are isolated yields.

Instruments

^{1}H and ^{13}C NMR spectra were recorded on a Bruker AVANCE III 400 spectrometer. High-resolution mass spectra (HRMS) were measured on a Bruker Apex IV instrument. UV-Vis spectra were obtained on a SHIMADZU UV-3600 spectrophotometer. Fluorescence experiments were performed on a HITACHI F-7000 (700 V PMT voltage). Excitation wavelength was recorded at 310 nm. 10 nm slit width was used for excitation and emission slits in the DMF system, while in the DCM/EA system, 10 nm slit width was used for excitation and 20 nm for emission. Circular dichroism (CD) spectra were obtained on JASCO J-815. Scanning electron microscopy (SEM) was performed using a JSM-7610F with 10 kV acceleration voltage. Samples were prepared by dropping the diluted gel onto a clean foil, followed by drying in air. A thin layer of Au was deposited onto samples before examination.

Differential scanning calorimetry (DSC) was performed using a Perkin-Elmer DSC7 calibrated for temperature and enthalpy changes. Samples were scanned twice from 0 to 210 °C and data were collected. The phase transition temperatures were taken at the peak temperatures in DSC thermograms with heating and cooling rates.

The mesomorphic properties of ***trans*-C$_n$-Chol** in the bulk state were observed by thermal polarizing optical microscopy (POM) using a Leitz Ortholux microscope equipped with a Mettler FP82 hot stage. The LC structures of ***trans*-C$_n$-Chol** in the solid state were studied at different temperature by small angle and wide angle X-ray scattering (WAXS and SAXS) using Cu Kα radiation (λ = 0.154 nm) from a 1.5 kW rotating anode generator. The diffraction patterns were recorded on photo-sensitive imaging plates.

Synthesis of TPE-OMe

TPE-OMe was synthesized according to the literature.[34] ^{1}H NMR (400 MHz, CDCl$_3$): δ = 7.17–7.03 (m, 15H, Ar*H*), 6.98–6.96 (d, *J* = 8.00 Hz, 2H, Ar*H*), 6.68–6.65 (d, *J* = 12.00 Hz, 2H, Ar*H*), 3.75 (s, 3H, OC*H$_3$*); ^{13}C NMR (100 MHz, CDCl$_3$): δ = 158.2, 144.2, 144.1, 140.7, 140.2, 136.3, 132.7, 131.5, 127.8, 127.7, 126.5, 126.4, 113.2, 55.2.

Synthesis of TPE-C$_6$-Br

TPE-C$_6$-Br was synthesized according to the literature.[35] ^{1}H NMR (400 MHz, CDCl$_3$): δ = 7.14–7.01 (m, 15H, Ar*H*), 6.94–6.92 (d, 2H, *J* = 8.00 Hz, Ar*H*), 6.64–6.62 (d, 2H, *J* = 8.00 Hz, Ar*H*), 3.90–3.87 (t, 2H, *J$_1$* = 4.00 Hz, *J$_2$* = 8.00 Hz, OC*H$_2$*), 3.44–3.41 (t, 2H, *J$_1$* = 8.00 Hz, *J$_2$* = 4.00 Hz, C*H$_2$*Br), 1.93–1.86 (m, 2H, C*H$_2$*), 1.79–1.73 (m, 2H, C*H$_2$*), 1.50–1.48 (m, 4H, 2C*H$_2$*); ^{13}C NMR (100 MHz, CDCl$_3$): δ = 151.7, 144.2, 144.1, 140.7, 140.1, 136.1, 132.6, 131.5, 127.8, 127.7, 126.5, 126.3, 113.7, 67.6, 33.9, 32.8, 29.3, 28.1, 25.5.

Synthesis of *trans*-azophenol

***trans*-Azophenol** was synthesized according to the literature.[36] ^{1}H NMR (400 MHz, DMSO-*d$_6$*): δ = 10.10 (s, 2H, Ar*OH*), 7.72–7.70 (d, 4H, *J* = 8.00 Hz, Ar*H*), 6.91–6.89 (d, 4H, *J* = 8.00 Hz, Ar*H*); ^{13}C NMR (100 MHz, DMSO-*d$_6$*): δ = 160.0, 145.2, 124.1, 115.8.

Synthesis of Br-C$_n$-Chol

The synthesis of **Br-C$_n$-Chol** will be described in detail based on the synthesis of a representative compound **Br-C$_5$-Chol**. Cholesterol (5.05 g, 13.06 mmol), 6-bromohexanoic acid (3.07 g, 15.68 mmol), 1-(3-dimethylaminopropyl)-3-ethylcarbodiimide hydrochloride (EDCI, 3.50 g, 18.28 mmol) and 4-dimethylaminopyridine (DMAP, 2.20 g, 18.28 mmol) were dissolved in DCM (185 mL). The mixture was stirred for 12 h at room temperature, and washed with 1 M HCl aqueous solution, water and saturated NaCl aqueous, respectively. After combining the organic phase, it was dried with anhydrous Na$_2$SO$_4$, filtered, concentrated under reduced pressure, and purified by column chromatography (hexane/EA = 5/1, v/v) to give a white solid.

Br-C$_1$-Chol. Yield: 15%. ^{1}H NMR (400 MHz, CDCl$_3$): δ = 5.40–5.38 (d, 1H, *J* = 8.00 Hz, Chol-6-C*H*), 4.74–4.66 (m, 1H, Chol-3-C*H*), 4.03 (s, 2H, C*H$_2$*Br), 2.37–2.35 (d, 2H, *J* = 8.00 Hz, Chol-4-C*H*), 1.02 (s, 3H, C*H$_3$*), 0.92–0.91 (d, 3H, *J* = 4.00 Hz, C*H$_3$*), 0.87–0.85 (d, 6H, *J* = 8.00 Hz, 2C*H$_3$*), 0.68 (s, 3H, C*H$_3$*); ^{13}C NMR (100 MHz, CDCl$_3$): δ = 166.9, 139.3, 123.3, 76.3, 56.8, 50.1, 42.5, 41.4, 39.9, 39.7, 38.0, 37.0, 36.7, 36.3, 35.9, 32.0, 28.4, 28.2, 27.7, 24.4, 24.0, 23.0, 22.7, 21.2, 19.4, 18.9, 12.0.

Br-C$_3$-Chol. Yield: 51%. ^{1}H NMR (400 MHz, CDCl$_3$): δ = 5.38–5.37 (d, 1H, *J* = 4.00 Hz, Chol-6-C*H*), 4.66–4.58 (m, 1H, Chol-3-C*H*), 3.48–3.45 (t, 2H, *J$_1$* = 4.00 Hz, *J$_2$* = 8.00 Hz, C*H$_2$*Br), 2.49–2.46 (t, 2H, *J$_1$* = 8.00 Hz, *J$_2$* = 4.00 Hz, C*H$_2$*COO), 2.33–2.31 (d, 2H, *J* = 8.00 Hz, Chol-4-C*H*), 1.02 (s, 3H, C*H$_3$*), 0.92–0.91 (d, 3H, *J* = 4.00 Hz, C*H$_3$*), 0.87–0.85 (m, 6H, 2C*H$_3$*), 0.68 (s, 3H, C*H$_3$*); ^{13}C NMR (100 MHz, CDCl$_3$): δ = 172.1, 139.7, 122.9, 74.4, 56.8, 56.3, 50.2, 42.5, 39.9, 39.7, 38.3, 37.1, 36.7, 36.3, 35.9, 33.0, 32.9, 32.1, 32.0, 28.4, 28.2, 28.0, 27.9, 24.4, 24.0, 23.0, 22.7, 21.2, 19.5, 18.9, 12.0.

Br-C$_5$-Chol. Yield: 63%. ^{1}H NMR (400 MHz, CDCl$_3$): δ = 5.38–5.37 (d, 1H, *J* = 4.00 Hz, Chol-6-C*H*), 4.66–4.58 (m, 1H, Chol-3-C*H*), 3.43–3.39 (t, 2H, *J$_1$* = 8.00 Hz, *J$_2$* = 8.00 Hz, C*H$_2$*Br), 2.32–2.28 (m, 4H, C*H$_2$*, and Chol-4-C*H*), 1.02 (s, 3H, C*H$_3$*), 0.92–0.91 (d, 3H, *J* = 4.00 Hz, C*H$_3$*), 0.87–0.85 (m, 6H, 2C*H$_3$*), 0.68 (s, 3H, C*H$_3$*); ^{13}C NMR (100 MHz, CDCl$_3$): δ = 173.0, 139.8, 122.8, 74.0, 56.8, 56.3, 50.2, 42.5, 39.9, 39.7, 38.3, 37.1, 36.7, 36.3, 36.9, 34.6, 33.7,

32.6, 32.1, 32.0, 28.4, 28.2, 28.0, 27.8, 24.4, 24.3, 24.0, 23.0, 22.7, 21.2, 19.5, 18.9, 12.0.

Synthesis of *trans*-TPE-C$_6$-azophenol

trans-azophenol (0.89 g, 4.15 mmol) and **TPE-C$_6$-Br** (1.72 g, 3.46 mmol) were dissolved in MeCN (150 mL), and then K$_2$CO$_3$ (0.80 g, 5.79 mmol) was added. The mixture was stirred at 85 °C for 24 h, and afterwards the reaction was cooled to room temperature and filtered. The filtrate was concentrated and further purified by column chromatography (hexane/EA = 3/1, v/v) to give an orange solid, *trans*-TPE-C$_6$-azophenol (yield 40%). ^{1}H NMR (400 MHz, CDCl$_3$): δ = 7.87–7.82 (t, 4H, J_1 = 8.00 Hz, J_2 = 12.00 Hz, ArH), 7.13–6.91 (m, 21H, ArH), 6.64–6.62 (d, 2H, J = 8.00 Hz, ArH), 5.01 (s, H, OH), 4.06–4.03 (t, 2H, J_1 = 8.00 Hz, J_2 = 4.00 Hz, CH_2O), 3.91–3.88 (t, 2H, J_1 = 4.00 Hz, J_2 = 8.00 Hz, OCH_2), 1.86–1.77 (m, 4H, CH_2), 1.55–1.53 (m, 4H, CH_2); ^{13}C NMR (100 MHz, CDCl$_3$): δ = 161.3, 157.8, 157.7, 147.4, 147.0, 144.2, 140.7, 140.1, 136.1, 132.7, 131.5, 127.8, 127.7, 126.5, 126.3, 124.7, 124.5, 115.9, 114.8, 113.7, 68.3, 67.8, 29.4, 29.3, 26.0.

Synthesis of *trans*-C$_0$-Chol

K$_2$CO$_3$ (0.32 g, 2.32 mmol) was added into a solution of cholesteryl chloroformate (0.98 g, 2.17 mmol) and *trans*-TPE-C$_6$-azophenol (1.00 g, 1.55 mmol) in DMF (50 mL) under argon, and then the mixture was stirred for 24 h at 50 °C. After cooling to room temperature, the reaction mixture was concentrated under reduced pressure to give an orange solid. The solid was re-dissolved in DCM (30 mL), and the organic phase was extracted with water. The organic phase was then collected, dried with anhydrous Na$_2$SO$_4$, filtered, concentrated under reduced pressure, and purified by recrystallization with EA to afford an orange crystal, *trans*-C$_0$-Chol (yield 53%). ESI-HRMS (+): C$_{72}$H$_{85}$O$_5$N$_2$ calc. 1057.6453 [M + H]$^+$, found 1057.6456; ^{1}H NMR (400 MHz, CDCl$_3$): δ = 7.92–7.89 (dd, 4H, J_1 = 4.00 Hz, J_2 = 4.00 Hz, J_3 = 4.00 Hz, ArH), 7.34–7.31 (d, 2H, J = 12.00 Hz, ArH), 7.14–6.99 (m, 17H, ArH), 6.93–6.91 (d, 2H, J = 8.00 Hz, ArH), 6.64–6.62 (d, 2H, J = 8.00 Hz, ArH), 5.44–5.43 (d, 1H, J = 4.00 Hz, Chol-6-CH), 4.65–4.57 (m, 1H, Chol-3-CH), 4.07–4.04 (t, 2H, J_1 = 8.00 Hz, J_2 = 4.00 Hz, CH_2-OAr), 3.92–3.89 (t, 2H, J_1 = 8.00 Hz, J_2 = 4.00 Hz, ArOCH_2), 2.55–2.45 (m, 2H, CH_2), 1.06 (s, 3H, CH_3), 0.93–0.92 (d, 3H, J = 4.00 Hz, CH_3), 0.88–0.86 (m, 6H, 2CH_3), 0.69 (s, 3H, CH_3); ^{13}C NMR (100 MHz, CDCl$_3$): δ = 161.9, 157.7, 152.8, 152.6, 150.5, 146.9, 144.2, 144.1, 140.7, 140.1, 139.2, 136.1, 132.7, 131.5, 127.8, 127.7, 126.5, 126.3, 124.9, 123.8, 123.4, 121.7, 114.9, 113.7, 79.2, 68.3, 67.7, 56.8, 56.3, 50.1, 42.5, 39.9, 39.7, 38.1, 37.0, 36.7, 36.3, 35.9, 32.1, 32.0, 29.4, 29.3, 28.4, 28.2, 27.8, 26.0, 24.4, 24.0, 23.0, 22.7, 21.2, 19.4, 18.9, 12.0.

Synthesis of *trans*-C$_n$-Chol (*n* = 1, 3, 5)

The synthesis of *trans*-C$_n$-Chol will be described in detail based on the synthesis of a representative compound *trans*-C$_5$-Chol. **Br-C$_5$-Chol** (0.73 g, 1.29 mmol) and *trans*-TPE-C$_6$-azophenol (0.99 g, 1.55 mmol) were dissolved in DMF (50 mL), and then K$_2$CO$_3$ (0.40 g, 2.58 mmol) was added. After stirring at 50 °C for

24 h, the reaction mixture was cooled to room temperature and concentrated under reduced pressure to afford an orange solid. The solid was re-dissolved in DCM (30 mL), and the organic phase was extracted with water. The organic phase was then collected, dried with anhydrous Na$_2$SO$_4$, filtered, concentrated under reduced pressure, and purified by recrystallization with EA to give an orange solid.

trans-C$_1$-Chol. Yield: 64%. ESI-HRMS (+): C$_{73}$H$_{87}$O$_5$N$_2$ calc. 1071.6609 [M + H]$^+$, found 1071.6605; ^{1}H NMR (400 MHz, CDCl$_3$): δ = 7.89–7.86 (m, 4H, ArH), 7.15–6.98 (m, 19H, ArH), 6.94–6.91 (d, 2H, J = 12.00 Hz, ArH), 6.64–6.62 (d, 2H, J = 8.00 Hz, ArH), 5.40–5.39 (d, 1H, J = 4.00 Hz, Chol-6-CH), 4.81–4.73 (m, 1H, Chol-3-CH), 4.67 (s, 2H, OCH_2COO), 4.06–4.03 (t, 2H, J_1 = 8.00 Hz, J_2 = 4.00 Hz, CH_2-OAr), 3.92–3.89 (t, 2H, J_1 = 8.00 Hz, J_2 = 4.00 Hz, ArOCH_2), 2.38–2.36 (d, 2H, J = 8.00 Hz, Chol-4-CH), 1.02 (s, 3H, CH_3), 0.93–0.91 (d, 3H, J = 8.00 Hz, CH_3), 0.88–0.86 (m, 6H, 2CH_3), 0.68 (s, 3H, CH_3); ^{13}C NMR (100 MHz, CDCl$_3$): δ = 168.1, 161.4, 159.8, 157.7, 147.8, 147.0, 144.2, 144.1, 140.7, 140.1, 139.3, 136.1, 132.6, 131.5, 127.8, 127.7, 126.5, 126.3, 124.6, 124.4, 123.2, 115.0, 114.8, 113.7, 75.5, 68.3, 67.7, 65.8, 56.8, 56.3, 50.1, 42.5, 39.9, 39.7, 38.1, 37.0, 36.7, 36.3, 35.9, 32.0, 29.4, 29.3, 28.4, 28.2, 27.8, 26.0, 24.4, 24.0, 23.0, 22.7, 21.2, 19.4, 18.9, 12.0.

trans-C$_3$-Chol. Yield: 42%. ESI-HRMS (+): C$_{75}$H$_{91}$O$_5$N$_2$ calc. 1099.6922 [M + H]$^+$, found 1099.6919; ^{1}H NMR (400 MHz, CDCl$_3$): δ = 7.87–7.85 (d, 4H, J = 8.00 Hz, ArH), 7.14–6.97 (m, 19H, ArH), 6.93–6.91 (d, 2H, J = 8.00 Hz, ArH), 6.64–6.62 (d, 2H, J = 8.00 Hz, ArH), 5.38–5.37 (d, 1H, J = 4.00 Hz, Chol-6-CH), 4.68–4.61 (m, 1H, Chol-3-CH), 4.10–4.02 (m, 4H, CH_2-OAr), 3.91–3.88 (t, 2H, J_1 = 4.00 Hz, J_2 = 8.00 Hz, OCH_2), 2.54–2.50 (t, 2H, J_1 = 8.00 Hz, J_2 = 8.00 Hz, CH_2COO), 2.33–2.32 (d, 2H, J = 4.00 Hz, Chol-4-CH), 1.02 (s, 3H, CH_3), 0.92–0.91 (d, 3H, J = 4.00 Hz, CH_3), 0.88–0.86 (m, 6H, 2CH_3), 0.68 (s, 3H, CH_3); ^{13}C NMR (100 MHz, CDCl$_3$): δ = 172.7, 161.3, 161.0, 157.7, 147.2, 147.1, 144.2, 144.1, 140.7, 140.1, 139.8, 136.1, 132.7, 131.5, 127.8, 127.7, 126.5, 126.3, 124.5, 122.8, 114.8, 113.7, 77.4, 74.3, 68.3, 67.7, 67.2, 56.8, 56.3, 50.2, 42.5, 39.9, 39.7, 38.3, 37.1, 36.8, 36.3, 35.9, 32.1, 32.0, 31.2, 29.4, 29.3, 28.4, 28.2, 28.0, 26.0, 24.8, 24.4, 24.0, 23.0, 22.7, 21.2, 19.5, 18.9, 12.0.

trans-C$_5$-Chol. Yield: 69%. ESI-HRMS (+): C$_{77}$H$_{95}$O$_5$N$_2$ calc. 1127.7235 [M + H]$^+$, found 1127.7231; ^{1}H NMR (400 MHz, CDCl$_3$): δ = 7.87–7.85 (d, 4H, J = 8.00 Hz, ArH), 7.13–6.97 (m, 19H, ArH), 6.93–6.91 (d, 2H, J = 8.00 Hz, ArH), 6.64–6.62 (d, 2H, J = 8.00 Hz, ArH), 5.38–5.37 (d, 1H, J = 4.00 Hz, Chol-6-CH), 4.66–4.59 (m, 1H, Chol-3-CH), 4.06–4.02 (t, 4H, J_1 = 8.00 Hz, J_2 = 8.00 Hz, 2CH_2O), 3.91–3.88 (t, 2H, J_1 = 4.00 Hz, J_2 = 8.00 Hz, OCH_2), 2.35–2.31 (m, 4H, CH_2), 1.01 (s, 3H, CH_3), 0.92–0.91 (d, 3H, J = 4.00 Hz, CH_3), 0.88–0.86 (d, 6H, 2CH_3), 0.67 (s, 3H, CH_3); ^{13}C NMR (100 MHz, CDCl$_3$): δ = 173.1, 161.2, 157.7, 147.1, 144.2, 144.2, 140.7, 140.1, 139.8, 136.1, 132.6, 131.5, 127.8, 127.7, 126.5, 126.3, 124.4, 122.8, 114.8, 113.7, 77.4, 74.0, 68.3, 68.1, 67.7, 56.8, 56.3, 50.2, 42.5, 39.9, 39.7, 38.3, 37.1, 36.7, 36.3, 35.9, 34.7, 32.1, 32.0, 29.4, 29.3, 29.0, 28.4, 28.2, 28.0, 26.0, 25.7, 24.9, 24.4, 24.0, 23.0, 22.7, 21.2, 29.5, 18.9, 12.0.

2252 | *Mater. Chem. Front.*, 2018, **2**, 2245–2253

This journal is © The Royal Society of Chemistry and the Chinese Chemical Society 2018

Conflicts of interest

There are no conflicts to declare.

Acknowledgements

Notes and references

1 N. M. Sangeetha and U. Maitra, *Chem. Soc. Rev.*, 2005, **34**, 821–836.

2 S. S. Babu, V. K. Praveen and A. Ajayaghosh, *Chem. Rev.*, 2014, **114**, 1973–2129.

3 S. Ghosh, V. K. Praveen and A. Ajayaghosh, *Annu. Rev. Mater. Res.*, 2016, **46**, 235–262.

4 C. Wang, Q. Chen, F. Sun, D. Zhang, G. Zhang, Y. Huang, R. Zhao and D. Zhu, *J. Am. Chem. Soc.*, 2010, **132**, 3092–3096.

5 N. Koumura, M. Kudo and N. Tamaoki, *Langmuir*, 2004, **20**, 9897–9900.

6 T. Wang, X. Yu, Y. Li, J. Ren and X. Zhen, *ACS Appl. Mater. Interfaces*, 2017, **9**, 13666–13675.

7 S. Panja, S. Bhattacharya and K. Ghosh, *Langmuir*, 2017, **33**, 8277–8288.

8 X. Pang, X. Yu, H. Lan, X. Ge, Y. Li, X. Zhen and T. Yi, *ACS Appl. Mater. Interfaces*, 2015, **7**, 13569–13577.

9 K. Murata, M. Aoki, T. Suzuki, T. Harada, H. Kawabata, T. Komori, F. Ohseto, K. Ueda and S. Shinkai, *J. Am. Chem. Soc.*, 1994, **116**, 6664–6676.

10 S. Sumiya, Y. Shiraishi and T. Hirai, *New J. Chem.*, 2013, **37**, 2642–2647.

11 J. T. van Herpt, J. Areephong, M. C. A. Stuart, W. R. Browne and B. L. Feringa, *Chem. – Eur. J.*, 2014, **20**, 1737–1742.

12 Z. Zhao, J. W. Y. Lam and B. Z. Tang, *Soft Matter*, 2013, **9**, 4564–4579.

13 M. Luo, S. Wang, M. Wang, S. Huang, C. Li, L. Chen and X. Ma, *Dyes Pigm.*, 2016, **132**, 48–57.

14 J. Yoshioka and F. Araoka, *Nat. Commun.*, 2018, **9**, 432–442.

15 A. Urbas, V. Tondiglia, L. Natarajan, R. Sutherland, H. P. Yu, J. H. Li and T. Bunning, *J. Am. Chem. Soc.*, 2004, **126**, 13580–13581.

16 V. Lisinetskii, A. Ryabchun, A. Bobrovsky and S. Schrader, *ACS Appl. Mater. Interfaces*, 2015, **7**, 26595–26602.

17 D. Garcia Velazquez, D. Diaz Diaz, A. Gutierrez Ravelo and J. Juan Marrero-Tellado, *Eur. J. Org. Chem.*, 2007, 1841–1845.

18 S.-Y. Kuo, C.-Y. Liu, R. Balamurugan, Y.-S. Zhang, S. Fitriyani and J. H. Liu, *New J. Chem.*, 2017, **41**, 15555–15563.

19 P. Xing, H. P. Tham, P. Li, H. Chen, H. Xiang and Y. Zhao, *Adv. Sci.*, 2018, **5**, 1700552.

20 P. Hanczyc, A. Justyniarski, D. A. Gedefaw, M. R. Andersson, M. Samoc and C. Muller, *RSC Adv.*, 2015, **5**, 49363–49368.

21 S. G. Liu, N. Li, L. Han, L. J. Li, N. B. Li and H. Q. Luo, *Mater. Horiz.*, 2018, **5**, 454–460.

22 Y. Gao, J. Hao, J. Wu, X. Zhang, J. Hu and Y. Ju, *Langmuir*, 2016, **32**, 1685–1692.

23 J. Tong, Y. Wang, J. Mei, J. Wang, A. Qin, J. Z. Sun and B. Z. Tang, *Chem. – Eur. J.*, 2014, **20**, 4661–4670.

24 J. Wang, S. Wang, Y. Zhou, X. Wang and Y. He, *ACS Appl. Mater. Interfaces*, 2015, **7**, 16889–16895.

25 B. Wu, W. Wang, J. Wang, S. Li and Y. He, *Dyes Pigm.*, 2018, **157**, 290–297.

26 S. Guo, K. Matsukawa, T. Miyata, T. Okubo, K. Kuroda and A. Shimojima, *J. Am. Chem. Soc.*, 2015, **137**, 15434–15440.

27 S. W. Basuki, V. Schneider, T. Strunskus, M. Elbahri and F. Faupel, *ACS Appl. Mater. Interfaces*, 2015, **7**, 11257–11262.

28 P. Duan, Y. Li, L. Li, J. Deng and M. Liu, *J. Phys. Chem. B*, 2011, **115**, 3322–3329.

29 C. Lin, S. Maisonneuve, R. Metivier and J. Xie, *Chem. – Eur. J.*, 2017, **23**, 14996–15001.

30 M.-H. Li, P. Auroy and P. Keller, *Liq. Cryst.*, 2000, **27**, 1497–1502.

31 L. Jia, A. Cao, D. Lévy, B. Xu, P.-A. Albouy, X. Xing, M. Bowick and M.-H. Li, *Soft Matter*, 2009, **5**, 3446–3451.

32 L. Jia, M. Liu, A. Di Cicco, P.-A. Albouy, B. Brissault, J. Penelle, S. Boileau, V. Barbier and M.-H. Li, *Langmuir*, 2012, **28**, 11215–11224.

33 L. Zhou, D. Zhang, S. Hocine, A. Pilone, S. Trépout, S. Marco, C. Thomas, J. Guo and M.-H. Li, *Polym. Chem.*, 2017, **8**, 4776–4780.

34 M. Banerjee, S. J. Emond, S. V. Lindeman and R. Rathore, *J. Org. Chem.*, 2007, **72**, 8054–8061.

35 Q. Ye, D. Zhu, L. Xu, X. Lu and Q. Lu, *J. Mater. Chem. C*, 2016, **4**, 1497–1503.

36 A. Bergen, S. Rudiuk, M. Morel, T. Le Saux, H. Ihmels and D. Baigl, *Nano Lett.*, 2016, **16**, 773–780.

This journal is © The Royal Society of Chemistry and the Chinese Chemical Society 2018

Mater. Chem. Front., 2018, **2**, 2245–2253 | **2253**